2022 EAGE ANNUAL
83RD CONFERENCE & EXHIBITION
MADRID I SPAIN

ACOUSTIC PLANE-WAVE MARCHENKO MULTIPLE ELIMINATION APPLIED ON COMPLEX MARINE DATA

G.A. Meles[1], C. Reinicke[2], M. Dukalski[2], K. Wapenaar[3]

[1] University of Lausanne; [2] Aramco Overseas Company BV; [3] TU Delft

Summary

Marchenko redatuming retrieves Green's functions inside an unknown medium, by solving a set of coupled Marchenko equations, which are derived from an under-determined system of equation and two temporal truncations. To constrain the problem, two assumptions are made, which hold reasonably well for acoustic, but not for elastodynamic waves. First, an early part of the inverse transmission field is needed which can be estimated for sufficiently-simple acoustic cases, but remains hard to predict for elastic media without detailed overburden knowledge. Secondly, the scheme assumes temporal separability of up-going focusing and Green's functions, which holds for many acoustic media but easily fails in presence of elastic effects. The impact of the failure to meet these assumptions is a somewhat controllable problem in 1.5D media. Independently, in acoustic media one can use a time-only focusing to retrieve focusing functions which collapse to a single plane wave below the overburden. We apply this approach to elastic data from a very complex almost 1.5D medium. The numerical example shows that the plane-wave approach can also be combined with mitigation of failure to satisfy the aforementioned assumptions and the result could lead to a high-fidelity internal multiple-free image.

Acoustic plane-wave Marchenko multiple elimination applied on complex marine data

Introduction

Marchenko redatuming is a powerful technique that allows retrieving responses to virtual sources in the subsurface by calculating so-called focusing functions from reflection data (for a recent review see Wapenaar et al., 2021). Using focusing functions associated with point-source responses to *directly* retrieve a multiple-free image (Zhang and Staring, 2018) can be computationally expensive, because it requires repeating the process for numerous redatuming levels. Multiple-free images can also be retrieved by employing plane-wave focusing functions which is expected to reduce computational cost, but at the price of less illumination compared to Marchenko point-source methods (Meles et al., 2018). In general, Marchenko equations can be solved if virtual source responses and focusing functions are separable in the time domain, except for an overlap that must be predicted. For acoustic waves, this overlap is often as simple as a direct wave, assuming sufficiently widely-spaced and mildly-curved reflectors. Elastic media, however, support wave propagation via coupled modes that travel with significantly different velocities. Compared to the acoustic case, elastodynamic virtual responses and the corresponding focusing functions are much more likely to share a non-trivial temporal overlap (Wapenaar, 2014; Reinicke et al., 2020). For predominantly horizontally-layered media, this overlap grows with increasing (horizontal) ray-parameters. In addition, elastodynamic mode conversions are weak in the vicinity of, and vanish in the limit of zero-incidence. Hence, the resemblance between acoustic and elastodynamic reflection data tends to increase with decreasing ray-parameters. As a result, the impact of ignoring elastodynamic effects and the associated challenges are less severe for small ray-parameters. Plane-wave focusing offers the flexibility to initialize the focusing functions for a limited illumination where the assumptions of the Marchenko method are better met. Further enhancements can be achieved by dip-filtering the reflection data, i.e. reducing the maximum angle of incidence not only for the focusing condition but also for the reflection operator.

Plane-wave focusing can be of great value for seismic processing in regions where (1) the geology can be approximated with a 1.5-D assumption, (2) the data is plagued by strong internal multiples and (3) the data quality allows for pre-processing with high amplitude fidelity (typically marine data). Staring et al. (2021) applied the acoustic Marchenko method on marine data from a region that satisfies points (1) - (3). Next, Reinicke et al. (2021) used a synthetic model, representative for the regional geology, to demonstrate that, in this case, neglecting elastic effects only has minor impact on the final migration result. We continue this synthetic study to investigate the reliability of applying the acoustic plane-wave Marchenko method on elastodynamic reflection data.

Theory

In the following, we provide a brief overview of elastodynamic single-sided representation theorems using plane waves (for more details see Wapenaar, 2014; Meles et al., 2018). Consider a 3D lossless elastic medium bounded by a reflection-free surface $\partial \mathrm{D}_0$ at the top (vertical spatial coordinate $x_3 = 0$). Single-sided plane-wave representations can be written for acoustic and elastodynamic waves as,

$$\tilde{\mathbf{G}}^{-,+}(\mathbf{x}', \mathbf{p}_H, x_{3,f}, \omega) = \int_{\partial D_0} \mathbf{R}(\mathbf{x}', \mathbf{x}, \omega)\tilde{\mathbf{F}}^{+}(\mathbf{x}, \mathbf{p}_H, x_{3,f}, \omega)\mathrm{d}^2\mathbf{x} - \tilde{\mathbf{F}}^{-}(\mathbf{x}', \mathbf{p}_H, x_{3,f}, \omega), \quad (1)$$

$$\left(\tilde{\mathbf{G}}^{-,-}(\mathbf{x}', -\mathbf{p}_H, x_{3,f}, \omega)\right)^{*} = \int_{\partial D_0} \mathbf{R}^{*}(\mathbf{x}', \mathbf{x}, \omega)\tilde{\mathbf{F}}^{-}(\mathbf{x}, \mathbf{p}_H, x_{3,f}, \omega)\mathrm{d}^2\mathbf{x} - \tilde{\mathbf{F}}^{+}(\mathbf{x}', \mathbf{p}_H, x_{3,f}, \omega). \quad (2)$$

Here, variables in bold capital letters represent wavefields which are scalars for acoustic, and 3x3 matrices for elastodynamic waves. In the latter case, columns and rows are associated with sources and receivers for compressional and shear waves (for details see e.g. Reinicke et al., 2021). The superscripts denote down-(+) and an up-(-) going components of the Green's ($\tilde{\mathbf{G}}^{-,\pm}$) and focusing ($\tilde{\mathbf{F}}^{\pm}$) functions. For the Green's functions, the first and second superscripts are associated with the wavefield direction on the receiver- and source-side, respectively. Complex conjugation (time reversal) is denoted with a *. The reflection response $\mathbf{R}$ is a Green's function due to a source of the temporal frequency ω at $\mathbf{x} = (x_1, x_2, x_3)^T$ and a receiver at $\mathbf{x}'$ with $x_3 = x_3' = 0$. The focusing function is source-free and has a focusing location at $x_3 = x_{3,f}$. For the Green's and focusing functions, the source/focusing coordinate is separated in horizontal and vertical components with $\mathbf{x}_H = (x_1, x_2)^T$ and $x_{3,f}$ on ∂D_f (below ∂D_0). Moreover, a plane-wave decomposition is applied along the horizontal source/focusing locations,

$$\widetilde{\mathbf{G}}^{-,\pm}(\mathbf{x},\mathbf{p}_H,x_{3,f},\omega)=\int_{\partial D_f}\mathbf{G}^{-,\pm}(\mathbf{x},\mathbf{x}_{H,f},x_{3,f},\omega)\,\mathrm{e}^{\mathrm{j}\omega\mathbf{p}_H\mathbf{x}_{H,f}}\mathrm{d}^2\mathbf{x}_{H,f}, \quad (3)$$

$$\widetilde{\mathbf{F}}^{\pm}(\mathbf{x},\mathbf{p}_H,x_{3,f},\omega)=\int_{\partial D_f}\mathbf{F}^{\pm}(\mathbf{x},\mathbf{x}_{H,f},x_{3,f},\omega)\,\mathrm{e}^{\mathrm{j}\omega\mathbf{p}_H\mathbf{x}_{H,f}}\mathrm{d}^2\mathbf{x}_{H,f}, \quad (4)$$

where $\mathbf{p}_H=(p_1,p_2)^T$ is the horizontal ray-parameter. The plane-wave representations in Eqs. 1-2 form an underdetermined system of equations that can be solved if a separation operator exists that can remove the Green's functions from Eqs. 1-2. For the *acoustic* case, Meles et al. (2018) postulate that such an operator exists, and demonstrate its performance numerically. The (acoustic) separation operator is a point-symmetric time window based on the kinematics of a direct transmission response to a plane-wave source at ∂D_f recorded at ∂D_0. The existence of an equivalent separation operator $\boldsymbol{\Theta}_{\tilde{F}}$ for the *elastodynamic* case cannot be guaranteed due to mode conversions resulting in non-trivial temporal overlaps of the Green's ($\widetilde{\mathbf{G}}^{-,\pm}$) and focusing ($\widetilde{\mathbf{F}}^{\pm}$) functions (see Reinicke et al., 2020). However, for nearly 1.5-D media, elastic mode conversions exhibit relatively small amplitudes in the vicinity of zero-incidence (small ray-parameters $\mathbf{p}_H$). To increase the similarity with the acoustic case and reduce the impact of converted waves, dip-filtering can be applied to the reflection data $\mathbf{R}$ (da Costa Filho et al., 2017; Reinicke et al., 2021).

The focusing function $\tilde{\mathbf{F}}^{+}$can then be expressed in a compact form as follows (van der Neut et al., 2015),

$$\tilde{\mathbf{F}}^{+}=\sum_{k=0}^{\infty}\left((\boldsymbol{\Theta}_{\tilde{F}}\mathbf{R}^{*}\boldsymbol{\Theta}_{\tilde{F}}\mathbf{R})^{k}\tilde{\mathbf{F}}_{d}^{+}\right). \quad (5)$$

The wavefield $\tilde{\mathbf{F}}_{d}^{+}$ is an initial estimate of the focusing function, which, for simple acoustic cases, simplifies to an inverse of a directly transmitted wave and is often approximated by a time reversal of the direct transmission modeled in a smooth background model. For more realistic acoustic scenarios, the scheme can be augmented to also handle short-period multiples without additional prior knowledge (Dukalski et al., 2019). Elastic cases, however, still require a significant amount of additional prior knowledge to retrieve the focusing and Green's functions (Reinicke et al., 2020). Hence, in the following, we consider the acoustic, i.e. scalar, form of Eq. 5. After evaluating Eq. 5, we retrieve the upgoing focusing ($\tilde{\mathbf{F}}^{-}=\boldsymbol{\Theta}_{\tilde{F}}\mathbf{R}\tilde{\mathbf{F}}^{+}$) and the Green's ($\widetilde{\mathbf{G}}^{-,\pm}$) functions using Eqs. 1-2. A local reflectivity and an imaging condition can then be estimated via the (scalar) equations (Meles et al., 2018),

$$\tilde{\mathbf{r}}_{im}(\mathbf{x}_{H,f},x_{3,f},\mathbf{p}_H,x_{3,f},\omega)=\int_{D_0}\left(\mathbf{G}_{d}^{-,-}\right)^{*}(\mathbf{x}_{H,f},x_{3,f},\mathbf{x}',\omega)\widetilde{\mathbf{G}}^{-,+}(\mathbf{x}',\mathbf{p}_H,x_{3,f},\omega)\mathrm{d}^2\mathbf{x}', \quad (6)$$

$$\tilde{\mathbf{I}}(\mathbf{x}_{H,f},x_{3,f},\mathbf{p}_H,x_{3,f})=\int\ \tilde{\mathbf{r}}_{im}(\mathbf{x}_{H,f},x_{3,f},\mathbf{p}_H,x_{3,f},\omega)e^{i\omega\mathbf{x}_{H,f}\cdot\mathbf{p}_H}\,\mathrm{d}\,\omega, \quad (7)$$

where $\mathbf{G}_{d}^{-,-}$ is a propagator in a smooth background (P-wave) velocity model.

Given the remaining challenges of solving Eq. 5 for elastodynamic data, we propose applying the acoustic version of Eq. 5, together with the imaging condition in Eqs. 6-7, on marine data (a pressure-only component of a full elastic response). For comparison, we repeat the experiment using a fully acoustic version of the marine model.

Numerical experiment using complex elastodynamic data

We investigate the impact of Marchenko multiple elimination ignoring elastic effects using the synthetic elastic model shown in Fig. 1a (further details on the model can be found in Reinicke et al., 2021). This well-log based model is representative for the geology associated with the field data example by Staring et al. (2021) where internal multiples are an outstanding challenge. Due to the predominantly horizontally-layered geology, primaries and multiples cannot be easily distinguished based on their moveout in pre-stack gathers or their shape after migration. Moreover, multiples create complex interference patterns that can disguise low relief structures and stratigraphic traps, which are often of high interest.

By controlling the S-wave velocity (V_S) model, we compute acoustic ($V_S=0$ below the water bottom) and marine ($V_S\neq 0$ below the water bottom) reflection data (see Figs. 2a and 2c). Due to the large ratio between P- and S-wave velocities (≈ 2), the acoustic and marine reflection data show significant differences towards the edges of the wavenumber-frequency cone. Hence, we apply a wavenumber-

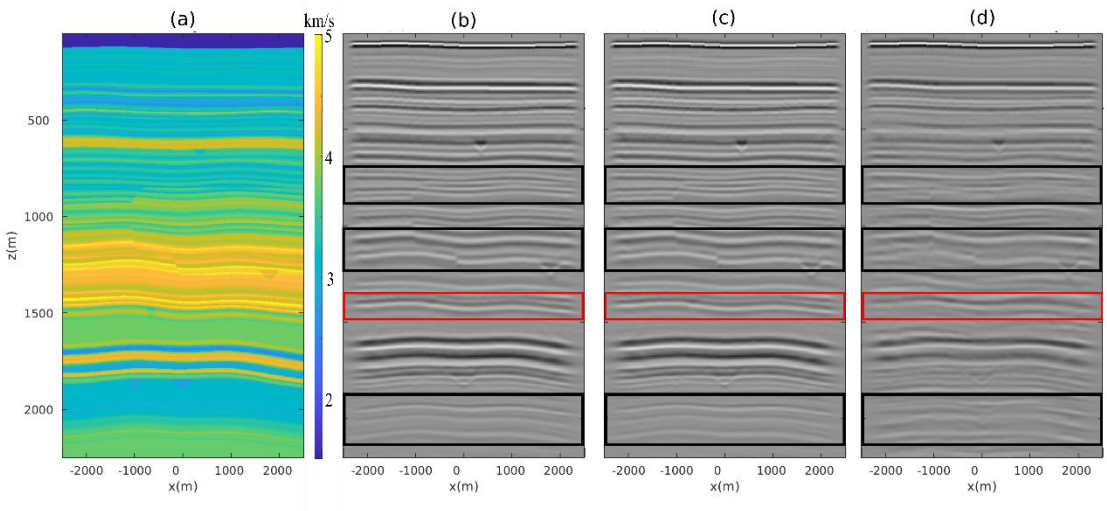

Figure 1 *(a) The model is parameterized by well-log based P- and S-wave velocities as well as density, all of which have identical geometries (only the P-wave model is shown). Migrated images of the plane-wave Marchenko demultiple results using (b) marine and (c) acoustic reflection data. (d) For comparison, we show the migrated image of the acoustic reflection data (i.e. without multiple elimination). Colored boxes highlight areas where both Marchenko results (marine & acoustic) improve the image quality (compared to the P-wave model). The Marchenko results derived from elastically modeled marine and acoustic data are nearly identical.*

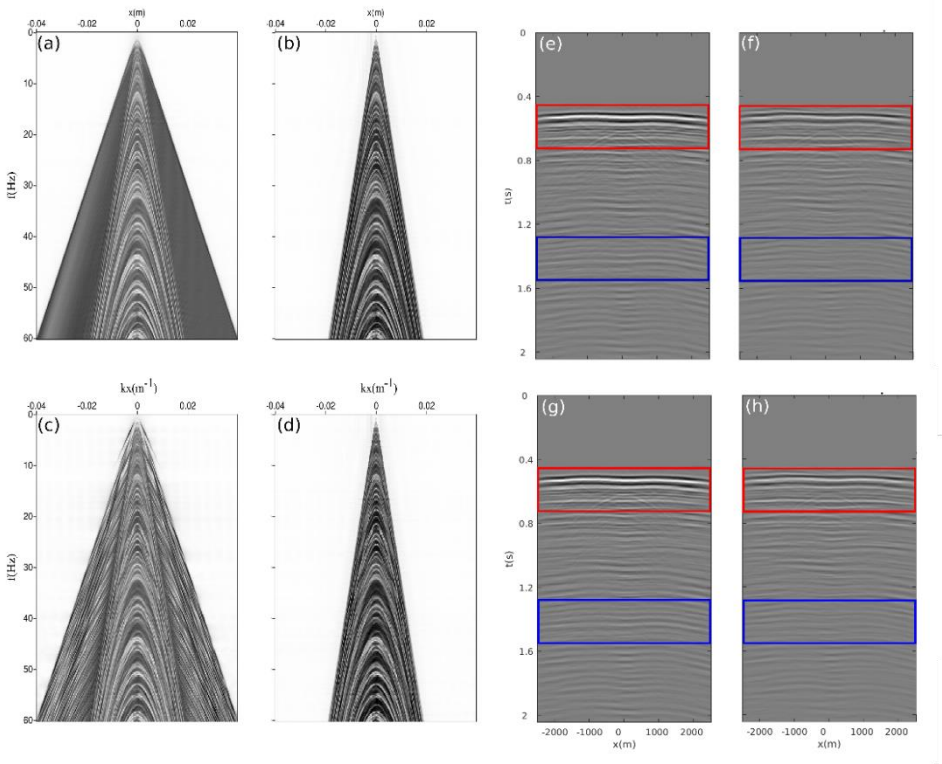

Figure 2 *Shot-gathers of the acoustic (a,b) and marine (c,d) reflection data before and after wavenumber-frequency filtering. Panels (e-f) respectively show the Green's function $\tilde{G}^{-,\pm}$ and the wavefield extrapolation result (i.e. without multiple elimination), both derived from acoustic reflection data for the focal depth $x_{3,f} = 1500m$. Panels (g-h) are analogous to (e-f) but derived from marine data. As in Fig.1, colored boxes highlight improvements due to multiple elimination and the low impact of ignoring elastic effects.*

frequency filter to reduce the elastic effects in the marine dataset (see Figs. 2b and 2d). Next, we use the acoustic and marine reflection data to evaluate 40 iterations of Eq. 5 using an initial focusing

function associated with a zero-incidence plane-wave ($\mathbf{p}_H = 0$). This algorithm is evaluated repeatedly for focusing depths associated with travel times ranging from 0s to 2s. The results are used to retrieve the Green's functions $\widetilde{\mathbf{G}}^{-,\pm}$ shown in Figs. 2e and 2g. To analyze the impact of the demultiple step, we apply wavefield extrapolation with $\left(\mathbf{G}_d^{-,-}\right)^*$ on the source-side of the reflection data (see Figs. 2f and 2h). Figs. 2e-h show significant differences between the wavefield extrapolation and the Marchenko results (see colored boxes). However, the impact of ignoring elastic effects in the marine data appears to be negligible for both the wavefield extrapolation as well as the Marchenko result. Subsequently, we evaluate Eqs. 6-7 using the acoustic and marine Marchenko results as well as the acoustic data after wavefield extrapolation (see Figs. 1b-d). A comparison to the P-wave velocity model demonstrates that the Marchenko results reveal structures that are otherwise hidden beneath multiple-borne artifacts. Moreover, migration seems to further reduce the impact of ignored elastic effects.

Conclusion

We investigated the reliability of acoustic plane-wave Marchenko imaging using marine instead of acoustic reflection data as input. For this study, we used an almost 1.5-D model that represents a region of interest. To minimize the impact of ignored elastic effects, we (1) applied a wavenumber-frequency filter and (2) initialized the Marchenko scheme with a zero-incidence plane wave. Our results show that the plane-wave Marchenko results provide images that are significantly closer to the velocity model than images derived from conventionally redatumed data (i.e. without multiple elimination). The Marchenko results derived from marine and acoustic reflection data are nearly identical, which increases our confidence of applying the acoustic plane-wave Marchenko method on properly filtered marine field data in the future. Follow-up work on the plane-wave Marchenko method will quantify the actual reduction of (a) computational costs and (b) quality due to the reduced illumination.

Acknowledgements

The work of K. Wapenaar was funded by the EU's Horizon 2020 research and innovation program (ERC grant 742703).

References

da Costa Filho, C. A., Meles, G. A., and Curtis, A. [2017] Elastic internal multiple analysis and attenuation using Marchenko and interferometric methods. Geophysics, 82(2):Q1-Q12.

Dukalski, M., Mariani, E., and de Vos, K. [2019] Handling short-period scattering using augmented Marchenko autofocusing. Geophysical Journal International, *216*(3), 2129-2133.

Meles, G. A., Wapenaar, K., and Thorbecke, J. [2018] Virtual plane-wave imaging via Marchenko redatuming. Geophysical Journal International, 214(1):508-519.

Reinicke, C., Dukalski, M., and Wapenaar, K. [2020] Comparison of monotonicity challenges encountered by the inverse scattering series and the Marchenko demultiple method for elastic waves. Geophysics, 85(5): Q11-Q26.

Reinicke, C., Dukalski, M., and Wapenaar, K. [2021] Internal multiple elimination: Can we trust an acoustic approximation? Geophysics, 86(5):1-44.

Staring, M., Dukalski, M., Belonosov, M., Baardman, R. H., Yoo, J., Hegge, R. F., van Borselen, R., and Wapenaar, K. [2021] Robust estimation of primaries by sparse inversion and Marchenko equation-based workflow for multiple suppression in the case of a shallow water layer and a complex overburden: A 2D case study in the Arabian Gulf. Geophysics 86.2: Q15-Q25.

van der Neut, J., Vasconcelos, I., and Wapenaar, K. [2015] On Green's function retrieval by iterative substitution of the coupled Marchenko equations. Geophysical Journal International, 203(2):792-813.

Wapenaar, K. [2014] Single-sided Marchenko focusing of compressional and shear waves. Physical Review E, 90(6):063202.

Wapenaar, K., Brackenhoff, J., Dukalski, M., Meles, G., Reinicke, C., Slob, E., Staring, M., Thorbecke, J., van der Neut, J. and Zhang, L. [2021] Marchenko redatuming, imaging and multiple elimination, and their mutual relations. Geophysics, 86.5: 1-103.

Zhang, L., and Staring, M. [2018] Marchenko scheme based internal multiple reflection elimination in acoustic wavefield. Journal of Applied Geophysics, 159, 429-433.